nature catalysis

SUPPLEMENTARY INFORMATION

https://doi.org/10.1038/s41929-018-0144-z

In the format provided by the authors and unedited.

Integrated tuneable synthesis of liquid fuels via Fischer–Tropsch technology

Jie Li[1,5], Yingluo He[1,5], Li Tan[1,5], Peipei Zhang[1,5], Xiaobo Peng[2]*, Anjaneyulu Oruganti[2], Guohui Yang[1,3], Hideki Abe[2], Ye Wang[4]* and Noritatsu Tsubaki[1]*

[1]Department of Applied Chemistry, School of Engineering, University of Toyama, Toyama, Japan. [2]National Institute for Materials Science, Tsukuba, Japan. [3]State Key Laboratory of Coal Conversion, Institute of Coal Chemistry, Chinese Academy of Sciences, Taiyuan, China. [4]State Key Laboratory of Physical Chemistry of Solid Surfaces, Collaborative Innovation Center of Chemistry for Energy Materials, College of Chemistry and Chemical Engineering, Xiamen University, Xiamen, China. [5]These authors contributed equally: Jie Li, Yingluo He, Li Tan, Peipei Zhang. *e-mail: PENG.Xiaobo@nims.go.jp; wangye@xmu.edu.cn; tsubaki@eng.u-toyama.ac.jp

Supplementary Table 1 | FT performance over the conventional supports and Y_{meso} zeolites.[a]

Catalyst		CO Conv. [%]	Hydrocarbon Selectivity [%][b]				C_{iso}/C_n[c]	$C_{olefins}$ [%][d]	CTY [mol_{CO} kg_{Co}^{-1} h^{-1}][e]
			CH_4	C_{2-4}	C_{5-20}	C_{21+}			
Co/SiO_2		47	8.8	4.4	64	23	0.6	18	155
Co/Al_2O_3		46	7.7	4.9	62	25	0.5	17	152
Co/Y_{micro}-Na		36	14	9.4	71	6.1	0.8	26	119
Co/Y_{meso}	Co/Y_{meso}-Na	32	11	5.4	72	12	0.7	24	106
	Co/Y_{meso}-H	28	17	19	64	0	2.2	12	93
	Co/Y_{meso}-Ce	34	11	6.6	82	0	2.3	18	112
	Co/Y_{meso}-La	40	9.5	4.5	86	0	3.3	17	132
	Co/Y_{meso}-Li	38	11	4.0	72	13	0.6	18	126
	Co/Y_{meso}-K	30	12	3.9	74	10	0.4	19	99

(**a**) Reaction conditions: T = 523 K; P = 2.0 MPa; H_2/CO = 1.0; flow rate, $W_{cat.}/F$ = 10 g h mol^{-1}; catalyst weight, 0.5 g; time on stream, 10 h. (**b**) The calculation of hydrocarbon selectivity based on the weight fraction of a product with respect to the total hydrocarbons. (**c**) C_{iso}/C_n is the ratio of isoparaffins to n-paraffins in C_{5-20}. (**d**) The olefins selectivity in C_{5-20}. (**e**) Cobalt-time-yield (CTY) represents moles of the converted CO over per kilogram of Co per hour.

Supplementary Table 2 | FT performance over Co/Y_{micro}-Na, Co/Y_{meso}-Na, Co/Y_{micro}-H and Co/Y_{meso}-H.[a]

Catalyst	CO Conv. [%]	Hydrocarbon Selectivity [%][b]				C_{iso}/C_n[c]
		CH_4	C_{2-4}	C_{5-20}	C_{21+}	
Co/Y_{micro}-Na	36	14	9.4	71	6.1	0.8
Co/Y_{meso}-Na	32	11	5.4	72	12	0.7
Co/Y_{micro}-H	30	23	26	51	0	2.7
Co/Y_{meso}-H	28	17	19	64	0	2.2

(**a**) Reaction conditions: T = 523 K; P = 2.0 MPa; H_2/CO = 1.0; flow rate, $W_{cat.}/F$ = 10 g h mol^{-1}; catalyst weight, 0.5 g; time on stream, 10 h. (**b**) The calculation of hydrocarbon selectivity based on the weight fraction of a product with respect to the total hydrocarbons. (**c**) C_{iso}/C_n is the ratio of isoparaffins to n-paraffins in C_{5-20}.

Supplementary Table 3 | Model reactions of n-C_{16} cracking over Co/Y_{micro}-Na, Co/Y_{meso}-Na, Co/Y_{micro}-H and Co/Y_{meso}-H.[a]

Catalyst	n-C_{16} Conv. [%]	Hydrocarbon Selectivity [%][b]			C_{iso}/C_n[c]
		CH_4	C_{2-4}	C_{5-15}	
Co/Y_{micro}-Na	90	23	3.0	74	0.01
Co/Y_{meso}-Na	93	15	1.4	84	0.02
Co/Y_{micro}-H	94	0.5	39	60	2.4
Co/Y_{meso}-H	97	1.9	25	73	2.1

(**a**) Reaction conditions: T = 523 K; H_2 pressure, 2.0 MPa; H_2 flow rate, 60 mL min^{-1}; n-C_{16} flow rate, 0.24 mL h^{-1}; catalyst weight, 0.5 g; time on stream, 10 h. (**b**) The calculation of hydrocarbon selectivity based on the weight fraction of a product with respect to the total hydrocarbons. (**c**) C_{iso}/C_n is the ratio of isoparaffins to n-paraffins in C_{5-15}.

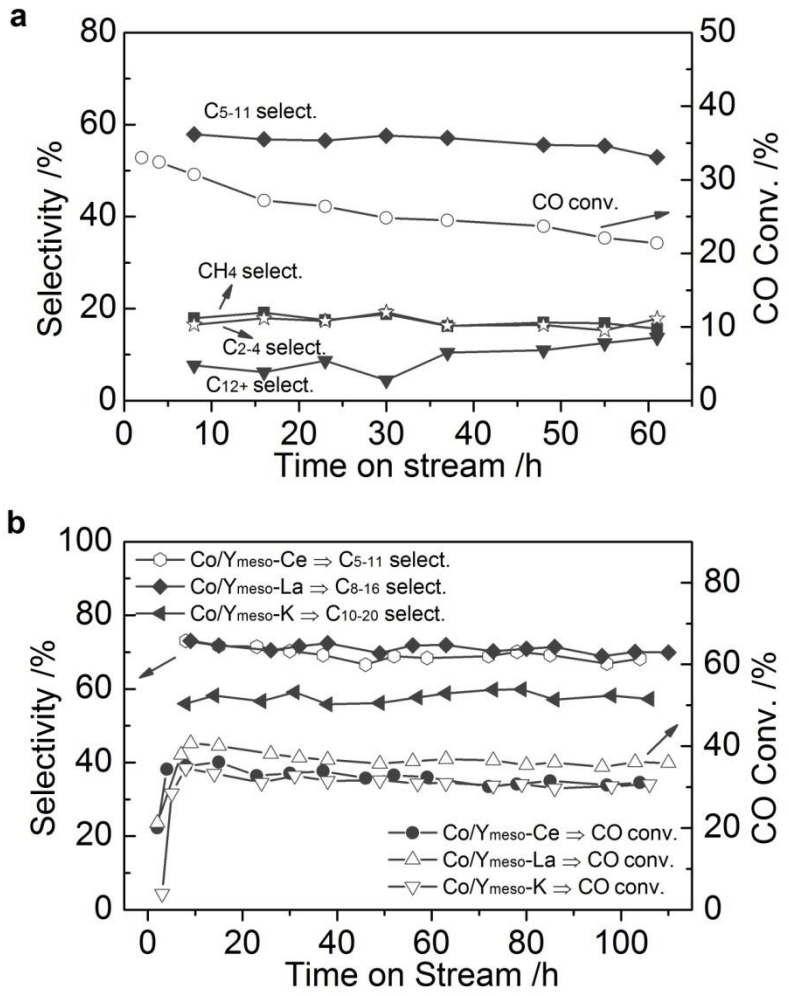

Supplementary Figure 1 | Time-on-stream evolution of CO conversion and fuel selectivity. (**a**) The stability for Co/Y_{meso}-H, (**b**) the stability for Co/Y_{meso}-Ce, Co/Y_{meso}-La and Co/Y_{meso}-K. Reaction conditions: T = 523 K; P = 2.0 MPa; H_2/CO = 1.0; flow rate, $W_{cat.}/F$ = 10 g h mol^{-1}; catalyst, 0.5 g.

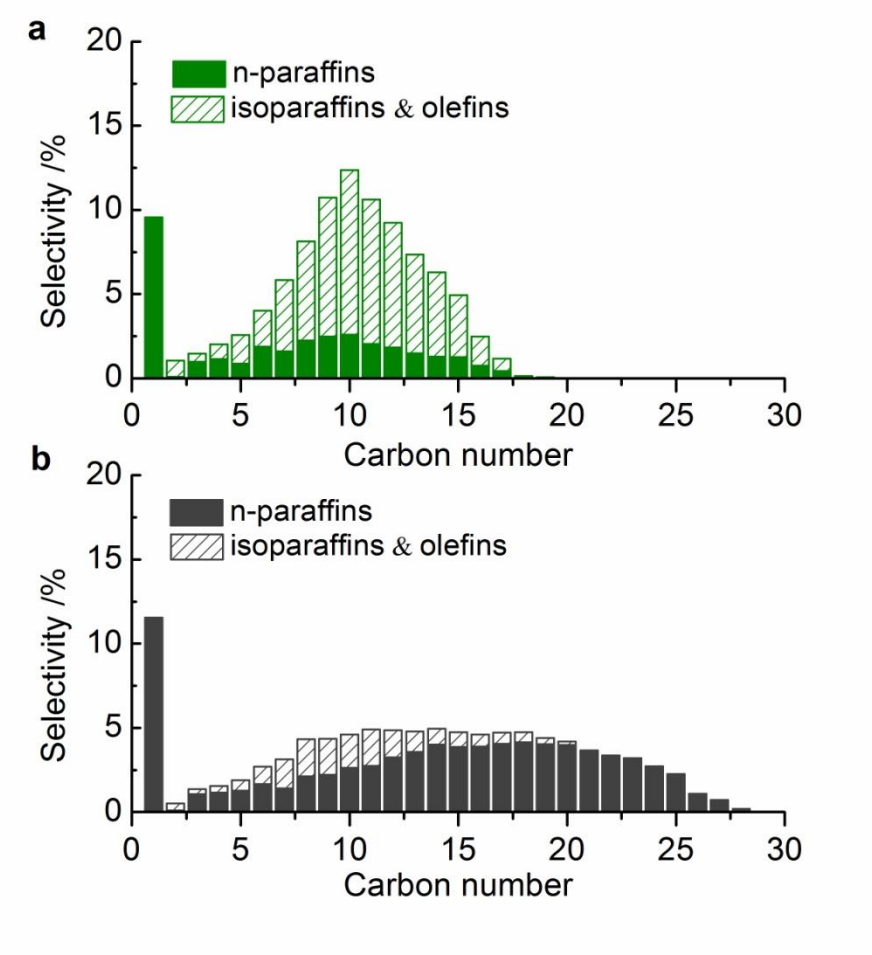

Supplementary Figure 2 | Comparison of FT product distribution over Co/Y_{meso}-La and Co/SiO_2-La. (**a**) Co/Y_{meso}-La, (**b**) Co/SiO_2-La. Reaction conditions: *T* = 523 K; *P* = 2.0 MPa; H_2/CO = 1.0; flow rate, $W_{cat.}$/F = 10 g h mol^{-1}; catalyst weight, 0.5 g; time on stream, 10 h. To prepare the catalyst of Co/SiO_2-La, the traditional SiO_2 support was used to replace the Y_{meso} zeolite in the preparation processes, while the other treatment conditions kept same.

Supplementary Table 4 | Comparison of research octane number (RON).

Synthesis Process	Research Octane Number (RON)
Hydrocracking of crude oils[a]	78~85
Traditional LTFT C_{5-11}[b]	35~43
Direct FT (Co/Y_{meso}-Ce)[c]	80

(**a**) The RON of Hydrocracking of crude oils was reproduced from ref. 1[1]. (**b**) The RON of traditional Low-Temperature FT synthesis (LTFT) was summarized from refs 2-4[2-4]. (**c**) The RON of direct FT synthesis over the Co/Y_{meso}-Ce was tested with PONA method by Nippon Oil Corporation (NOC) in Japan.

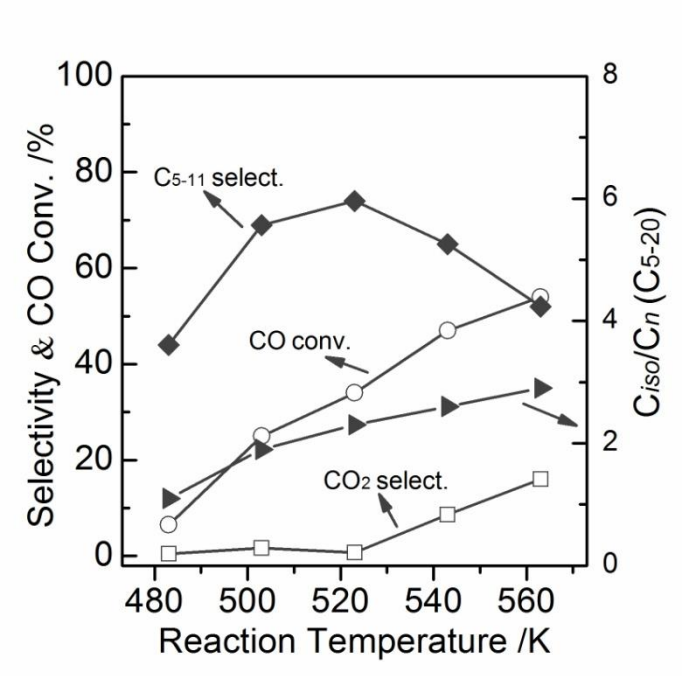

Supplementary Figure 3 | FT reactions over Co/Y_{meso}-Ce with different reaction temperature. Reaction conditions: T = 483 ~ 563 K; P = 2.0 MPa; H_2/CO = 1.0; flow rate, $W_{cat.}/F$ = 10 g h mol^{-1}; catalyst, 0.5 g. The Co/Y_{meso}-Ce exhibited low gasoline selectivity, when the reaction temperatures were too low or too high. The high gasoline selectivity with medium hydrocracking/isomerization was obtained at the reaction temperature of 523 K.

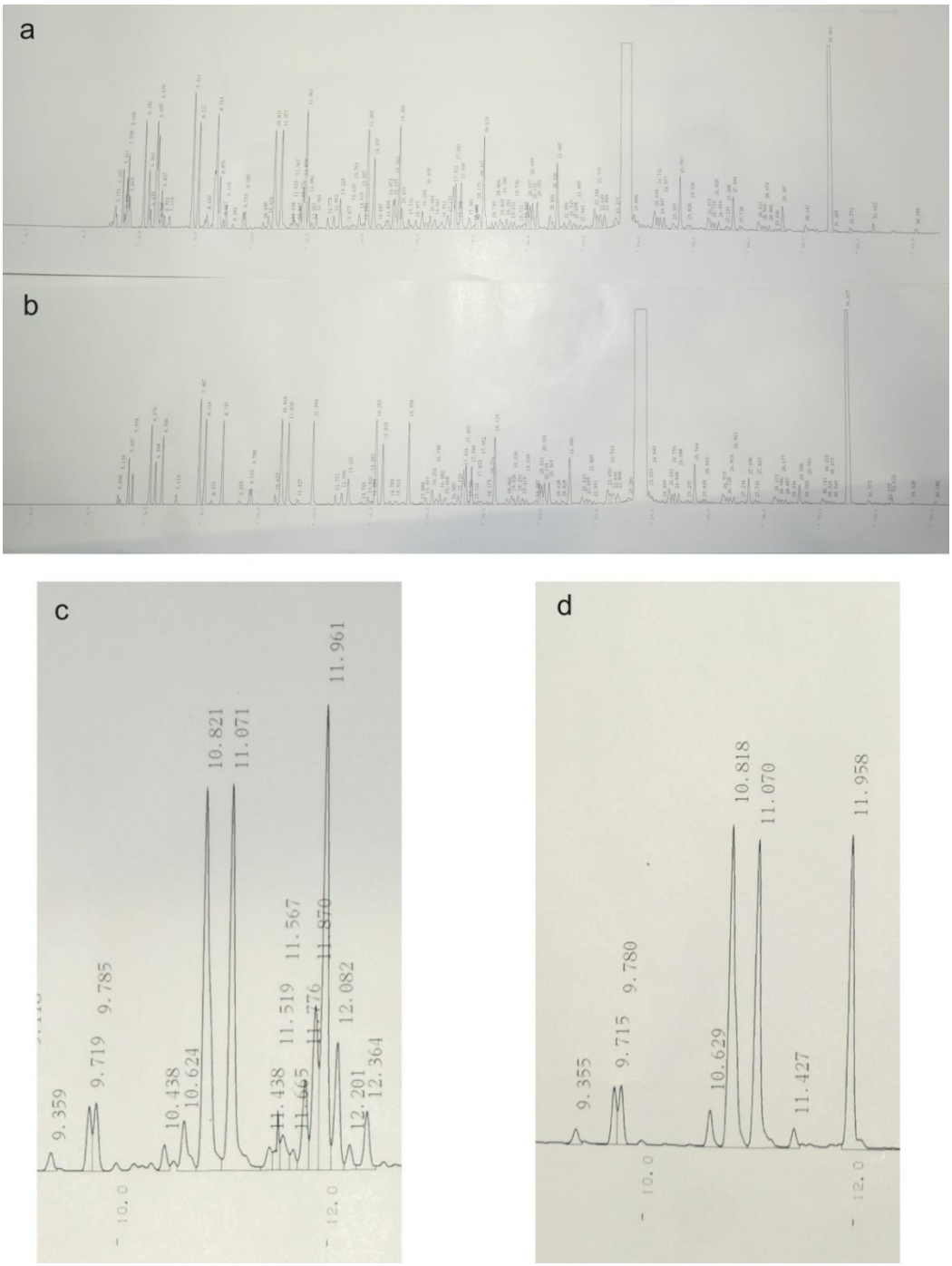

Supplementary Figure 4 | The detailed distributions of liquid fuel over the Co/Y_{meso}-Ce after direct FT process. (**a**) The liquid fuel from direct FT synthesis; (**b**) the liquid fuel after H_2SO_4 treatment; (**c**) the C_8 from direct FT process; (**d**) the C_8 after H_2SO_4 treatment. Reaction conditions were the same with Supplementary Table 1.

Supplementary Table 5 | Comparison of diesel fuel properties.

Diesel fuel property	Conventional diesel[a]	FT-GTL[b] (Shell International Gas Limited)	Direct FT[c] (Co/Y_{meso}-K)
Cetane Number (CN)	52	75	74
Density at 15 °C (g/cm^3)	0.84	0.78	0.78
90% distillation (T90, °C)	331	310	305
Flash point (°C)	/	/	91
Pour point (°C)	/	/	−20
Viscosity (mm^2/s)	2.67(40 °C)	2.74 (40 °C)	3.05 (30 °C)
Sulfur (ppm)	403	3	<1
Aromatics	27.7 wt%	1.4 wt%	<1vol%

(**a**) The diesel fuel properties of conventional diesel fuel were reproduced from ref. 5[5]. (**b**) The GTL-FT diesel fuel properties of the Shell International Gas Limited were reproduced from refs 5 and 6[5,6]. (**c**) The diesel fuel properties of direct FT synthesis over the Co/Y_{meso}-K were tested with JIS K2204 method by National Traffic Safety and Environment Laboratory (NTSEL) in Japan.

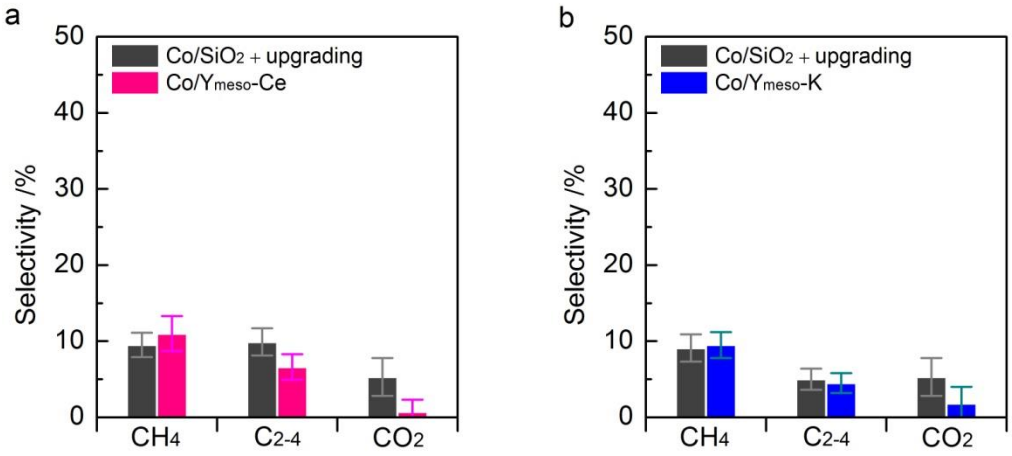

Supplementary Figure 5 | Comparison of direct FT synthesis and FT/upgrading on CH_4, C_{2-4} and CO_2. (**a**) The comparison of Co/Y_{meso}-Ce and FT/upgrading. The product selectivity from FT/upgrading based on FT synthesis on traditional Co/SiO_2 and the C_{12+} upgrading[7,8]. (**b**) The comparison of Co/Y_{meso}-K and FT/upgrading. The product selectivity from FT/upgrading based on FT synthesis on traditional Co/SiO_2 and the C_{21+} upgrading[9,10]. The results revealed that the selectivity of small molecule products did not significantly differ from the products in the multistep process of FT/upgrading. The distribution of the data values was represented by the mean value, which were obtained by multiple measurements. The error bar represented the standard deviation to uncover the overall distribution of the data.

Supplementary Table 6 | Textural properties of Y_{micro} and Y_{meso} samples.

Sample		A_{BET}[a] [$m^2 g^{-1}$]	A_{meso}[b] [$m^2 g^{-1}$]	V_{micro}[c] [$cm^3 g^{-1}$]	V_{meso}[d] [$cm^3 g^{-1}$]	D_{meso}[e] [nm]	D_{micro}[f] [nm]
Y_{micro}-Na		540	54	0.20	0.07	/	0.7
Y_{micro}-H		536	51	0.21	0.09	/	0.7
	Y_{meso}-Na	552	138	0.18	0.27	17	0.7
	Y_{meso}-H	504	126	0.14	0.25	14	0.7
Y_{meso}	Y_{meso}-Ce	515	103	0.17	0.19	21	0.7
	Y_{meso}-La	536	76	0.18	0.15	29	0.7
	Y_{meso}-K	512	99	0.16	0.20	25	0.7

(**a**) BET area; (**b**) BJH adsorption cumulative surface area of pores in 2-50 nm; (**c**) the micropore volume evaluated by the *t*-plot method; (**d**) the mesopore volume evaluated by the BJH method; (**e**) pore size for mesopores evaluated by the BJH method; (**f**) pore size for micropores estimated by the HK method.

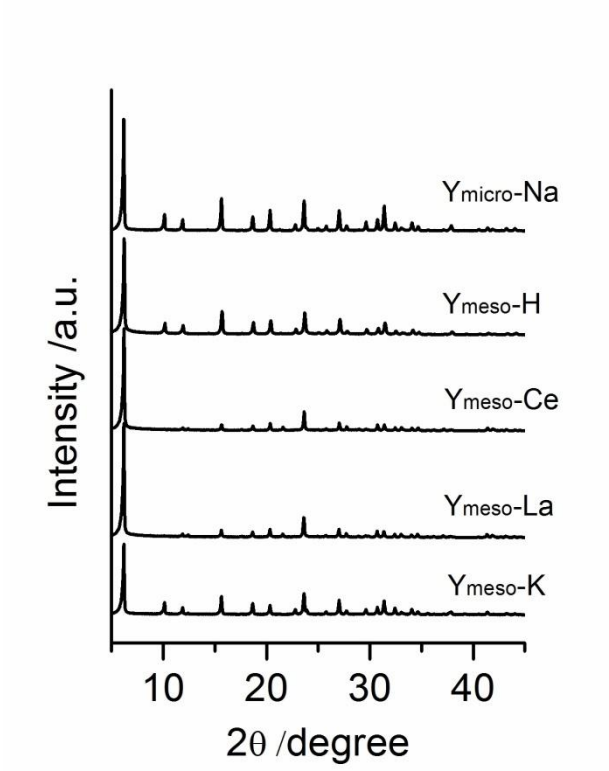

Supplementary Figure 6 | XRD patterns for the Y_{micro}-Na and Y_{meso} samples.

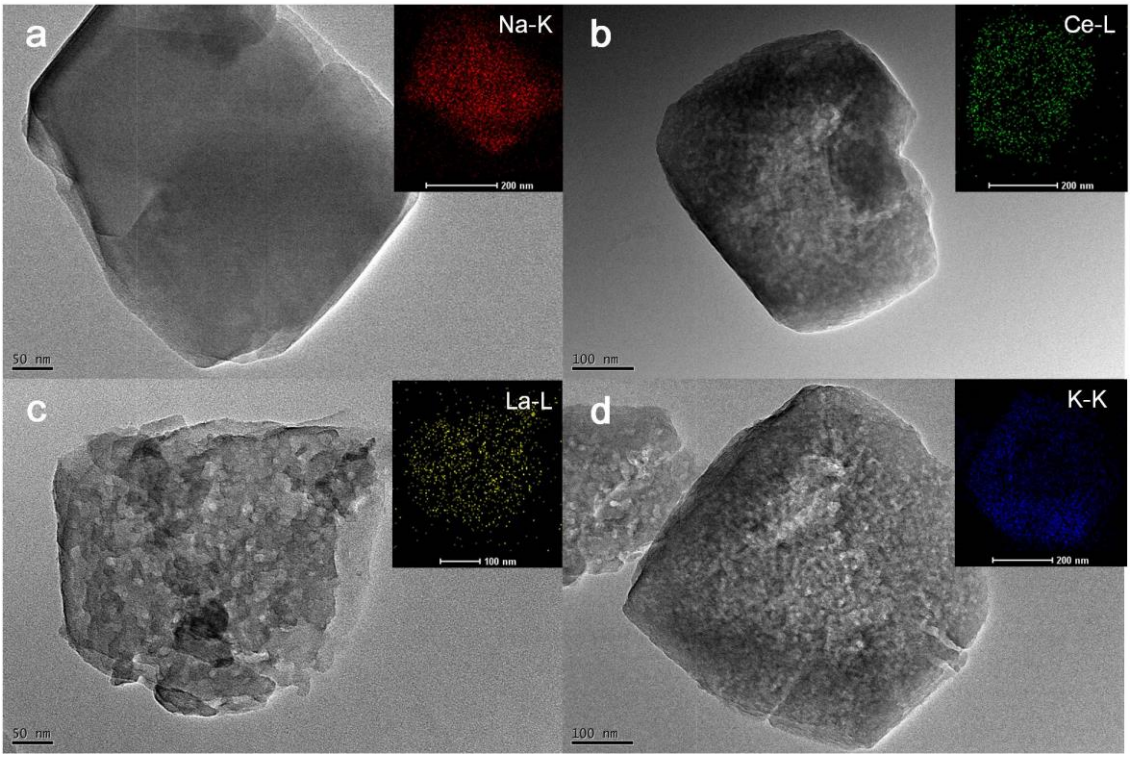

Supplementary Figure 7 | TEM and EDS results for the Y_{micro}-Na and Y_{meso} samples. (**a**) Y_{micro}-Na, (**b**) Y_{meso}-Ce, (**c**) Y_{meso}-La, (**d**) Y_{meso}-K. The scale bars of the TEM images for Y_{micro}-Na, Y_{meso}-Ce, Y_{meso}-La and Y_{meso}-K correspond to 50, 100, 50 and 100 nm, respectively. The scale bars of the EDS analysis for Y_{micro}-Na, Y_{meso}-Ce, Y_{meso}-La and Y_{meso}-K correspond to 200, 200, 100 and 200 nm, respectively. These results were obtained by using FEI Tecnai F20.

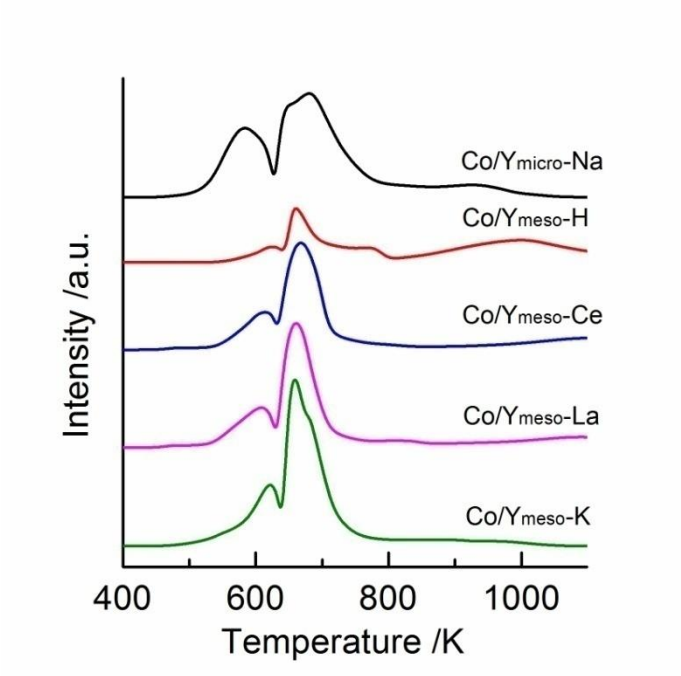

Supplementary Figure 8 | H_2-TPR profiles for Co/Y_{micro}-Na and Co/Y_{meso} samples.

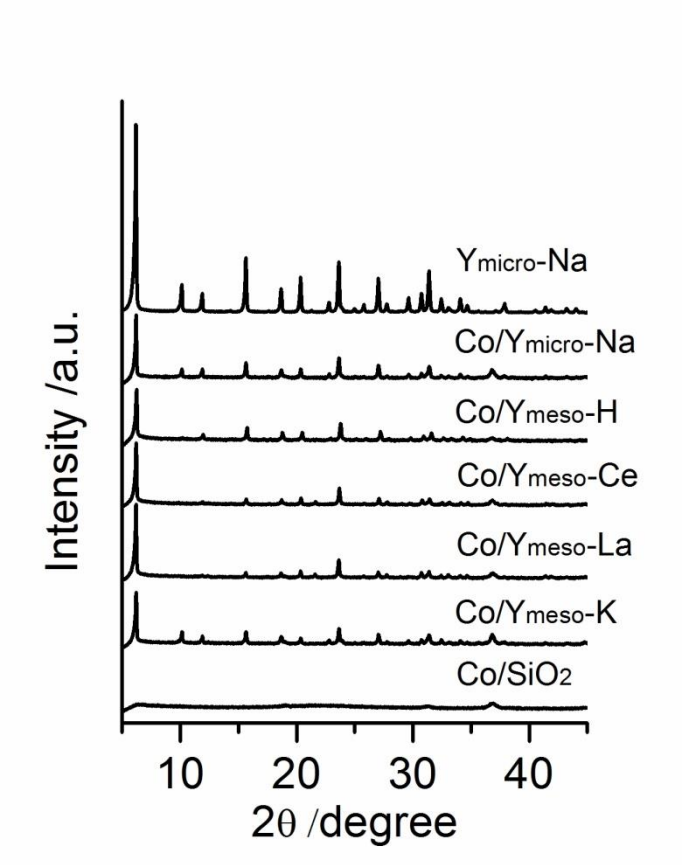

Supplementary Figure 9 | XRD patterns for the Co/Y_{meso} and other reference samples. The average size of cobalt oxide in the precursor catalysts was calculated by the Scherrer equation at $2\theta = 37^{o}$.

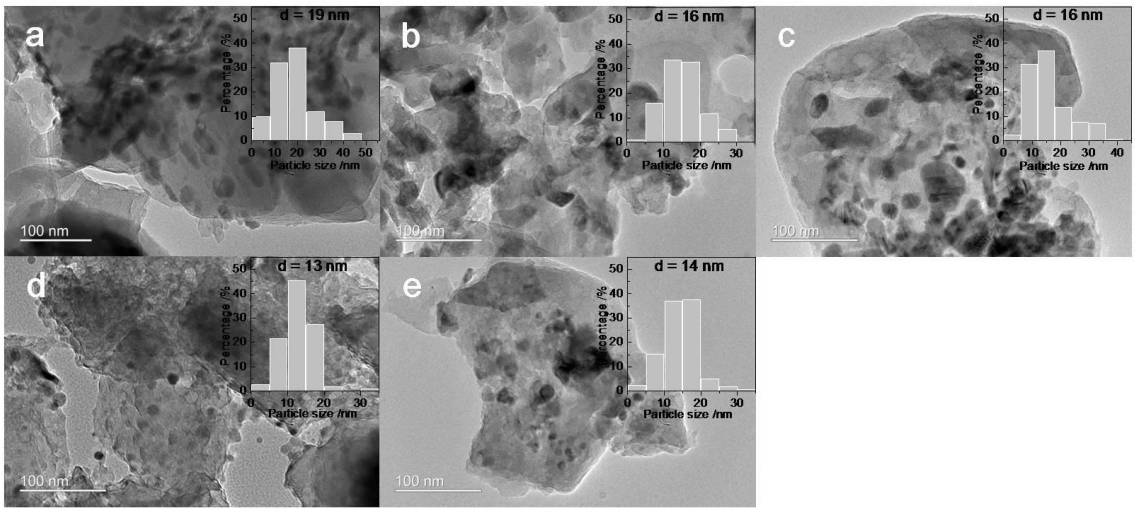

Supplementary Figure 10 | TEM and Co particle size distribution for the Co/Y_{micro}-Na and Co/Y_{meso} samples. (**a**) Co/Y_{micro}-Na, (**b**) Co/Y_{meso}-H, (**c**) Co/Y_{meso}-Ce, (**d**) Co/Y_{meso}-La, (**e**) Co/Y_{meso}-K. The morphology observation was obtained by using JEOL JEM-2100F2.

Supplementary Table 7 | Physicochemical properties for Co/Y_{micro}-Na, Co/Y_{meso}-H, Co/Y_{meso}-Ce, Co/Y_{meso}-La, Co/Y_{meso}-K and Co/SiO_2.

Sample	Reduction degree[a] [%]	H_2 chemisorption amount[b] [μmol g^{-1}]	Size of Co_3O_4[c] [nm]	Co dispersion[d] [%]	Co diameter[e] [nm]	Mean Co size[f] [nm]
Co/Y_{micro}-Na	77	64	22	6.5	15	19
Co/Y_{meso}-H	49	53	16	8.5	11	16
Co/Y_{meso}-Ce	70	72	19	8.1	12	16
Co/Y_{meso}-La	73	85	14	9.2	10	13
Co/Y_{meso}-K	80	76	17	7.5	13	14
Co/SiO_2	84	79	16	7.4	13	/

(**a**) Measured by the H_2-O_2 titration method; (**b**) evaluated from the H_2 chemisorption measurement; (**c**) calculated by the XRD at 2θ = 37°; (**d**) calculated from the H_2 chemisorption amount; (**e**) calculated using the following equation: Co diameter = 0.96/dispersion[11,12]; (**f**) evaluated from the TEM images.

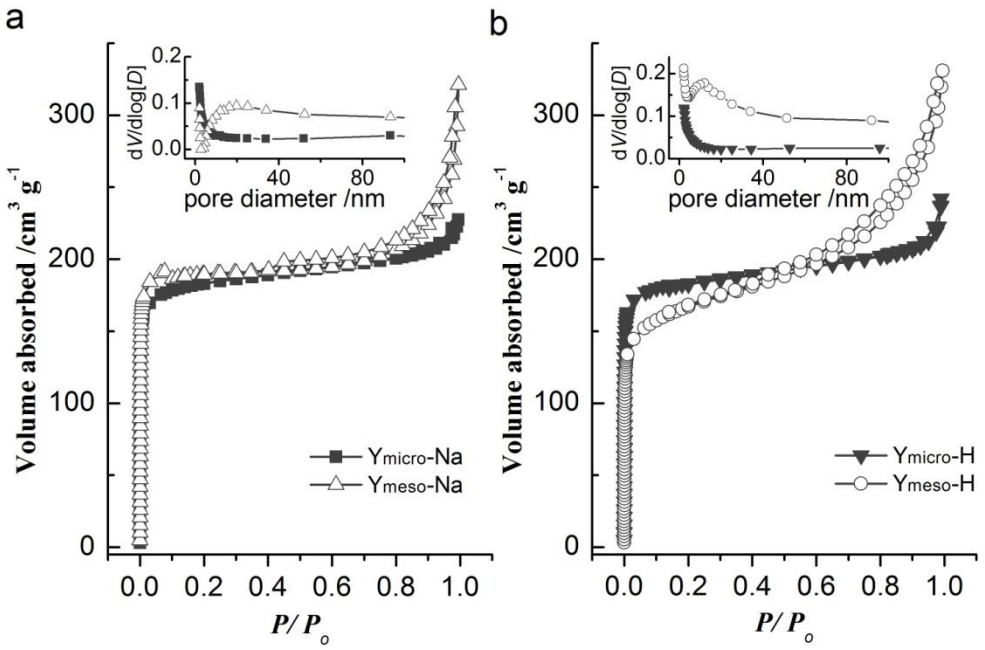

Supplementary Figure 11 | Ar adsorption-desorption isotherms and the pore-diameter distributions. (**a**) Y_{micro}-Na and Y_{meso}-Na, (**b**) Y_{micro}-H and Y_{meso}-H.

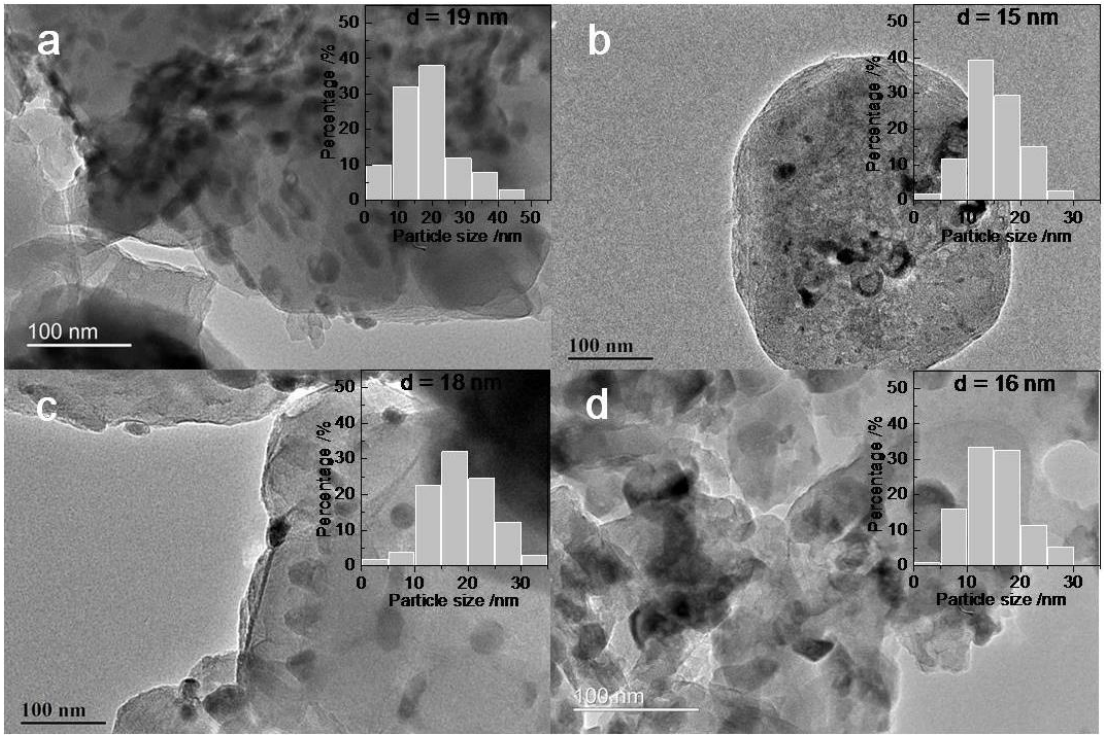

Supplementary Figure 12 | TEM and Co particle size distribution for Co/Y_{micro}-Na, Co/Y_{meso}-Na, Co/Y_{micro}-H and Co/Y_{meso}-H. (**a**) Co/Y_{micro}-Na, (**b**) Co/Y_{meso}-Na, (**c**) Co/Y_{micro}-H, (**d**) Co/Y_{meso}-H. The morphology observation of (**a**) and (**d**) was obtained by using JEOL JEM-2100F2 (National Institute for Materials Science, Japan). The morphology observation of (**b**) and (**c**) was obtained by using JEOL JEM-2100F (Institute of Coal Chemistry, Chinese Academy of Sciences, China).

Supplementary Table 8 | Physicochemical properties for Co/Y_{micro}-Na, Co/Y_{meso}-Na, Co/Y_{micro}-H and Co/Y_{meso}-H.

Sample	Reduction degree[a] [%]	H_2 chemisorption amount[b] [μmol g^{-1}]	Co dispersion[c] [%]	Co diameter[d] [nm]	Mean Co size[e] [nm]
Co/Y_{micro}-Na	77	64	6.5	15	19
Co/Y_{meso}-Na	79	91	9.0	11	15
Co/Y_{micro}-H	61	56	7.3	13	18
Co/Y_{meso}-H	49	53	8.5	11	16

(**a**) Measured by the H_2-O_2 titration method; (**b**) evaluated from the H_2 chemisorption measurement; (**c**) calculated from the H_2 chemisorption amount; (**d**) calculated using the following equation: Co diameter = 0.96/dispersion[11,12]; (**e**) evaluated from the TEM images.

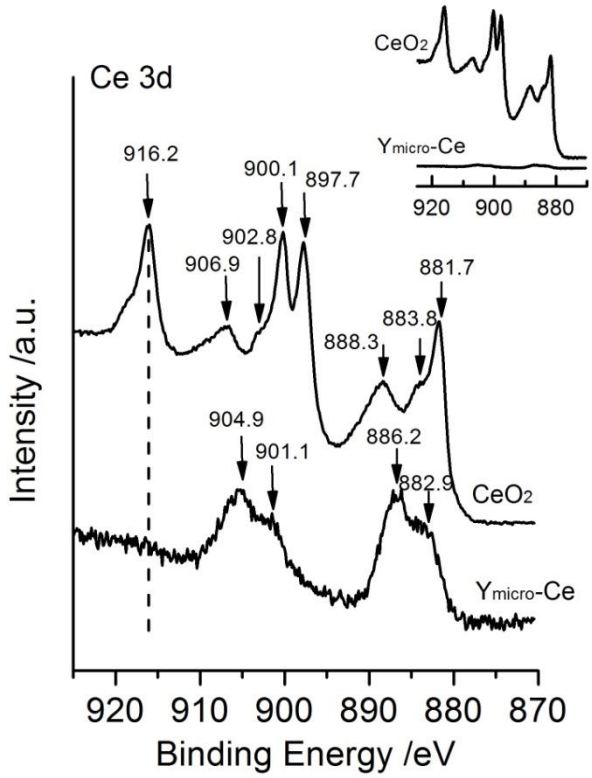

Supplementary Figure 13 | XPS spectra of Ce 3d for CeO_2 and Y_{micro}-Ce. The inset is the Ce 3d XPS at the same test conditions. To facilitate comparison, the peak intensity of CeO_2 was reduced by 20 times. For the CeO_2, the peaks of binding energies at 881.7, 883.8, 888.3 and 897.7 eV corresponded to Ce 3d5/2 and its satellite, respectively. The peaks at 900.1, 902.8, 906.9 and 916.2 eV were due to Ce 3d3/2 and its satellite[13,14]. For the Y_{micro}-Ce, the binding energies of 882.9 and 886.2 eV were assigned to Ce 3d5/2 and its satellite, and those at 901.1 and 904.9 eV corresponded to Ce 3d3/2 and its satellite. Typically, the Ce (IV) species showed a characteristic peak at 916.2 eV such as CeO_2. But the Y_{micro}-Ce had no obvious characteristic peak at 916.2 eV, and the peaks were similar with those of Ce 3d XPS of $Ce(NO_3)_3$[14], suggesting that the Ce ion remained trivalent in the Y_{micro}-Ce.

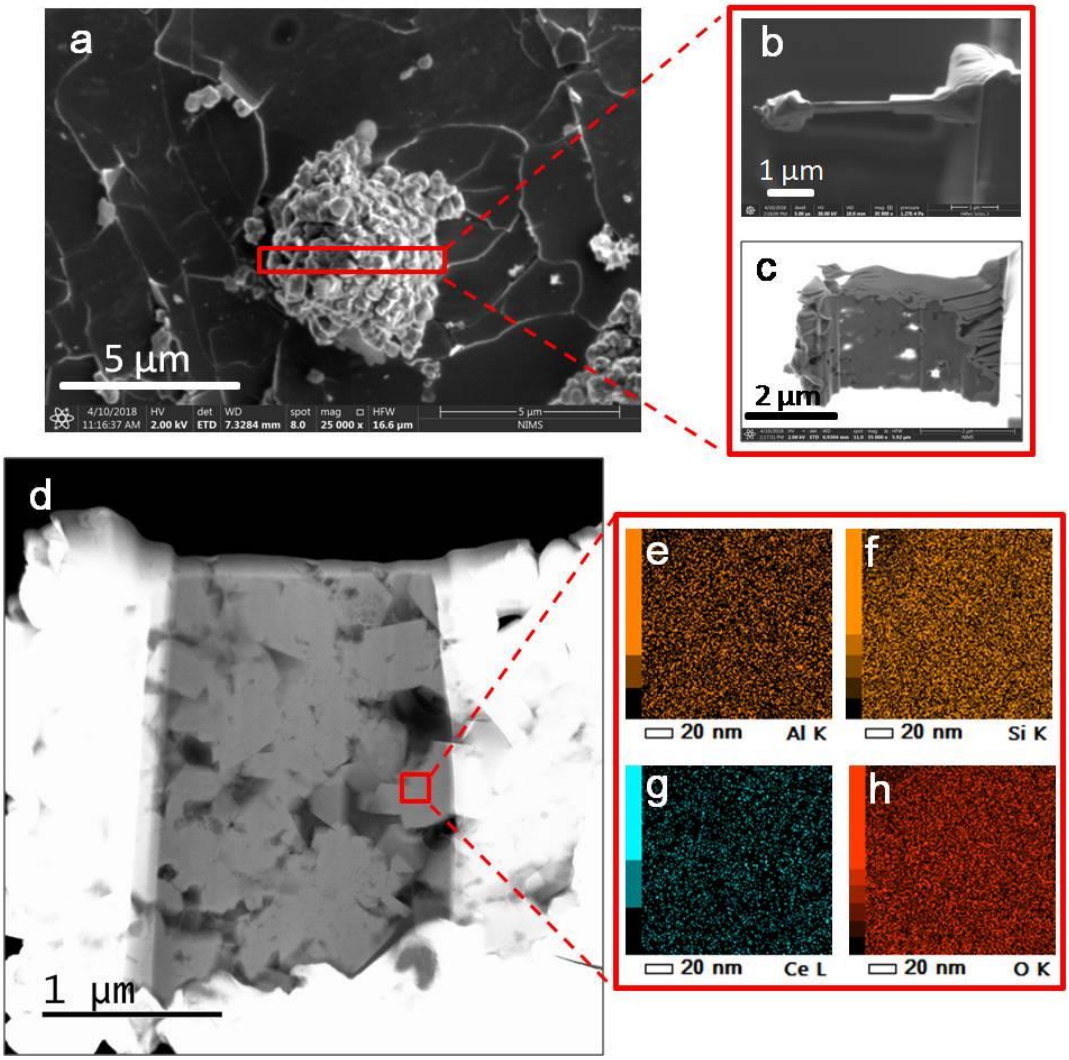

Supplementary Figure 14 | FIB-SEM and STEM results for the Y_{micro}-Ce. (**a**)-(**c**) SEM observation for FIB samples: (**a**) the accumulation from a number of Y_{micro}-Ce particles, (**b**) the Y_{micro}-Ce particles with thickness of 100 nm after FIB cutting, (**c**) the new cross-section of the Y_{micro}-Ce particles; (**d**) STEM for the new cross-section; (**e**)-(**h**) EDS analysis for Al, Si, Ce and O in a single Y_{micro}-Ce particle. Please note that original thickness of single particle of Y_{micro}-Ce was about 500-1000 nm.

Supplementary Table 9 | Effect of alkali metal ions added to Co/Y_{meso}-Na on FT activity.[a]

Catalyst[b]	Addition of Alkali [wt %]	Addition amount/Co [molar ratio]	Internal Na/Co [molar ratio]	CO Conv. [%]
Co/Y_{meso}-H	0	0	~ 0	28
Co/Y_{meso}-Na	0	0	1.4	32
Co-Li/Y_{meso}-Na	2	1.1	1.4	6.5
Co-Na/Y_{meso}-Na	2	0.3	1.4	15
Co-K/Y_{meso}-Na	2	0.2	1.4	20

(**a**) Reaction conditions: T = 523 K; P = 2.0 MPa; H_2/CO = 1.0; flow rate, $W_{cat.}/F$ = 10 g h mol^{-1}; catalyst weight, 0.5 g; time on stream, 10 h. (**b**) The loading of Co was 15 wt%. Alkali metal ions were added by co-melt infiltration with $Co(NO_3)_2 \cdot 6H_2O$ and the alkali metal nitrates. The Co/Y_{meso}-Na with internal Na/Co ratio of 1.4 did not influence the FT activity, compared with the Co/Y_{meso}-H. But the Co-Li/Y_{meso}-Na, prepared by extra Li addition with Li/Co ratio of 1.1, significantly decreased the FT activity.

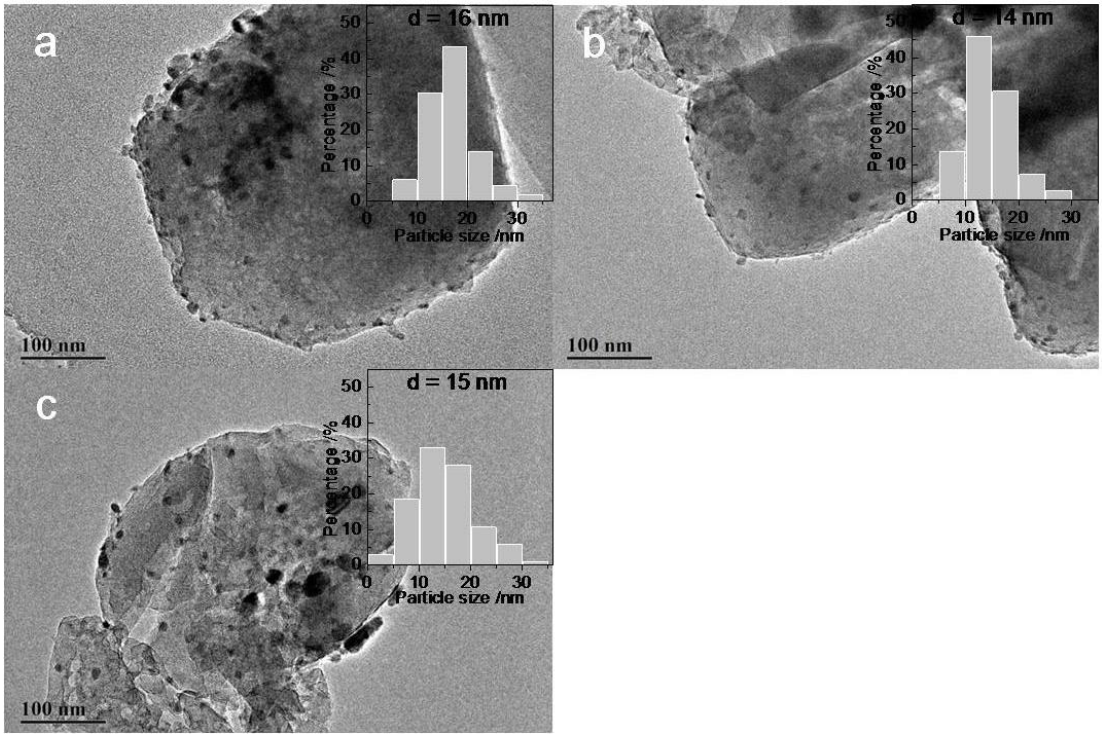

Supplementary Figure 15 | TEM and Co particle size distribution of Co/Y_{meso} samples after the FT reaction. (**a**) Co/Y_{meso}-Ce, (**b**) Co/Y_{meso}-La, (**c**) Co/Y_{meso}-K. The morphology observation was obtained by using JEOL JEM-2100F.

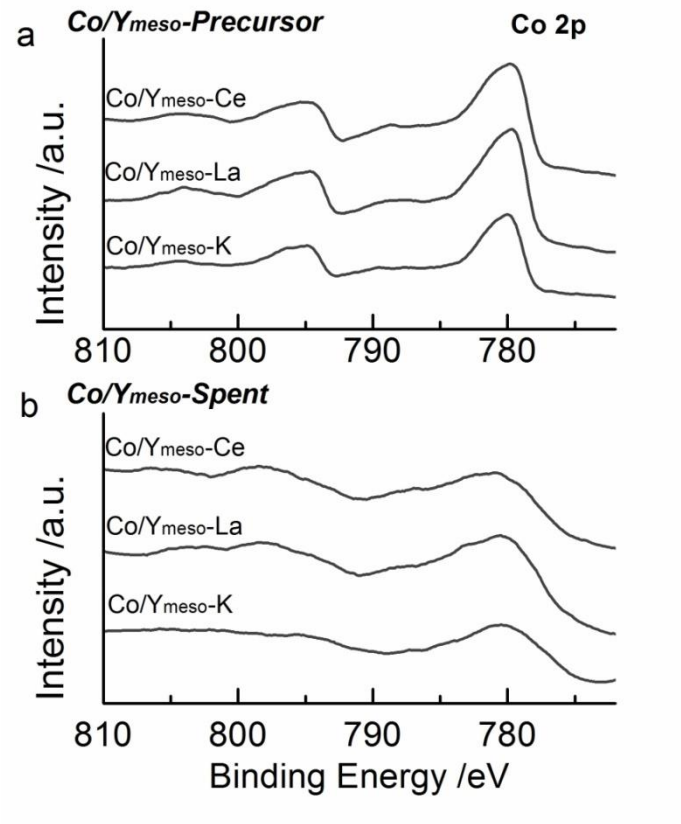

Supplementary Figure 16 | XPS spectra of Co 2p for Co/Y_{meso}-Precursor and Co/Y_{meso}-Spent. XPS results revealed two main components for Co 2p3/2, Co 2p1/2, and their satellites both on Co/Y_{meso}-Precursor and Co/Y_{meso}-Spent[15-17]. The peak of Co 2p3/2 in 780 eV region for the Co/Y_{meso}-Precursor was due to Co_3O_4. The same region for the Co/Y_{meso}-Spent exhibited a mixture of cobalt oxides and metallic cobalt. In addition, in the Co/Y_{meso}-Precursor or Co/Y_{meso}-Spent, the cobalt phases of Co/Y_{meso}-Ce, Co/Y_{meso}-La, and Co/Y_{meso}-K were very similar to each other.

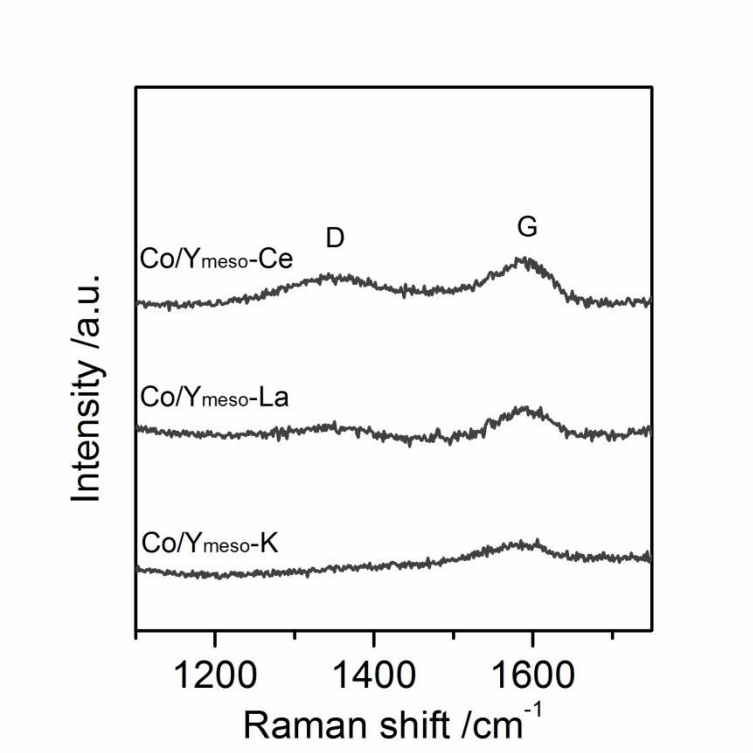

Supplementary Figure 17 | Raman spectra for Co/Y_{meso} after the FT synthesis of 10 h. The D band is associated with disordered structure of graphene. The G band is due to the first-order scattering of E_{2g} mode of sp^2 carbon domains. It arises from the stretching of the C-C bond in graphitic materials[18,19]. Although G bands were slightly higher than D bands in these samples, they all displayed very weak peak intensity, indicating very weak carbon accumulation on these used Co/Y_{meso} catalysts.

Supplementary Note. The calculation details for the bifunctional catalyst distribution model. n is the number of carbon atoms in a product; α is the chain growth probability, and β is the cracking contribution degree. *W*n is the weight fraction of a product with n number of carbon atoms; S_n is the selectivity to the product[20-23].

Supplementary Equations.

The calculation details for the gasoline distribution model as follows:

$$W_n = n\alpha^{n-1}(1-\alpha)^2 \quad (1)$$

$$W_{1\sim4} = \sum_{n=1}^{4}(n\alpha^{n-1}(1-\alpha)^2) \quad (2)$$

$$W_{5\sim11} = \sum_{n=5}^{11}(n\alpha^{n-1}(1-\alpha)^2) \quad (3)$$

$$W_{12+} = 1 - W_{1\sim4} - W_{5\sim11} \quad (4)$$

$$W_{5\sim11}' = W_{5\sim11} + \beta(1 - W_{1\sim4} - W_{5\sim11}) \quad (5)$$

$$W_{5\sim11}' = \beta + (1-\beta) * W_{5\sim11} - \beta * W_{1\sim4} \quad (6)$$

$$W_{5\sim11}{}' = \beta + (1-\beta) * \sum_{n=5}^{11}(n\alpha^{n-1}(1-\alpha)^2) - \beta * \sum_{n=1}^{4}(n\alpha^{n-1}(1-\alpha)^2) \quad (7)$$

$$S_{5\sim11}\ (\%) = W_{5\sim11}{}' * 100 \quad (8)$$

The calculation details for the jet fuel distribution model as follows:

$$W_{8\sim16}{}' = \beta + (1-\beta) * \sum_{n=8}^{16}(n\alpha^{n-1}(1-\alpha)^2) - \beta * \sum_{n=1}^{7}(n\alpha^{n-1}(1-\alpha)^2) \quad (9)$$

$$S_{8\sim16}\ (\%) = W_{8\sim16}{}' * 100 \quad (10)$$

The calculation details for the diesel fuel distribution model as follows:

$$W_{10\sim20}{}' = \beta + (1-\beta) * \sum_{n=10}^{20}(n\alpha^{n-1}(1-\alpha)^2) - \beta * \sum_{n=1}^{9}(n\alpha^{n-1}(1-\alpha)^2) \quad (11)$$

$$S_{10\sim20}\ (\%) = W_{10\sim20}{}' * 100 \quad (12)$$

Supplementary Table 10 | Calculation result for the β value of gasoline.

Sample	Hydrocarbon Selectivity [%]				C_{12+} Contribution degree (β)
	CH_4	C_{2-4}	C_{5-11}	C_{12+}	
Ideal ASF distribution	1.0	7.1	26	66	0.7
Co/Y_{meso}-Ce	11	6.6	74	8.6	

Due to weak cracking ability on the Co/SiO_2, the ideal ASF distribution of $\alpha = 0.9$ was obtained by supposing that the growth trend of hydrocarbons $C_{5–11}$ follows the original ASF model. The gasoline β value was calculated by the Supplementary Equations 7 and 8.

Supplementary Table 11 | Calculation result for the β value of jet fuel.

Sample	Hydrocarbon Selectivity [%]				C_{17+} Contribution degree (β)
	CH_4	C_{2-7}	C_{8-16}	C_{17+}	
Ideal ASF distribution	1.0	18	33	48	0.8
Co/Y_{meso}-La	9.6	17	72	1.4	

The jet fuel β value was calculated by the Supplementary Equations 9 and 10.

Supplementary Table 12 | Calculation result for the β value of diesel fuel.

Sample	Hydrocarbon Selectivity [%]					C_{21+} Contribution degree (β)
	CH_4	C_{2-4}	C_{5-9}	C_{10-20}	C_{21+}	
Ideal ASF distribution	1.0	7.1	18	37	36	0.6
Co/Y_{meso}-K	12	3.9	16	58	10	

The diesel fuel β value was calculated by the Supplementary Equations 11 and 12.

Supplementary Table 13 | Comparison of experimental liquid fuel distribution and model distribution.

Sample	Hydrocarbon Selectivity [%]		
	C_{5-11}	C_{8-16}	C_{10-20}
Ideal ASF distribution	26	33	37
Bifunctional catalyst distribution model	72	72	59
Experimental distribution	74[a]	72[b]	58[c]

(**a**) Gasoline selectivity over the Co/Y_{meso}-Ce; (**b**) jet fuel selectivity over the Co/Y_{meso}-La; (**c**) diesel fuel selectivity over the Co/Y_{meso}-K.

Supplementary References

1. Scherzer, J. & Gruia, A. J. Hydrocracking science and technology. *Marcel Dekker*, New York, (1996).
2. Klerk, A. de. Fischer-Tropsch refining. *Wiley-VCH*, Weinheim, (2011).
3. Klerk, A. de. Environmentally friendly refining: Fischer-Tropsch versus crude oil. *Green Chem.* **9**, 560-565 (2007).
4. Leckel, D. Diesel production from Fischer-Tropsch: the past, the present, and new concepts. *Energy Fuels* **23**, 2342-2358 (2009).
5. Wu, T. *et al.* Physical and chemical properties of GTL-diesel fuel blends and their effects on performance and emissions of a multicylinder DI compression ignition engine. *Energy Fuels* **21**, 1908-1914 (2007).
6. Abu-Jrai, A. *et al.* Effect of gas-to-liquid diesel fuels on combustion characteristics, engine emissions, and exhaust gas fuel reforming, comparative study. *Energy Fuels* **20**, 2377-2384 (2006).
7. Maxwell, I. E. Zeolite catalysis in hydroprocessing technology. *Catal. Today* **l,** 385-413 (1987).
8. Bouchy, C. *et al.* Fischer-Tropsch waxes upgrading via hydrocracking and selective hydroisomerization. *Oil & Gas Science and Technology. Rev. IFP*, **64**, 91-112 (2009).
9. Dry, M. E. The Fischer-Tropsch process: 1950–2000. *Catal. Today* **71**, 227-241 (2002).
10. Calemma, V. *et al.* Middle distillates from hydrocracking of FT waxes: Composition, characteristics and emission properties. *Catal. Today* **149**, 40-46 (2010).
11. Zowtiak, J. M. & Bartholomew, C. H. The kinetics of H_2 adsorption on and desorption from cobalt and the effects of support there on. *J. Catal.* **83**, 107-120 (1983).
12. Reuel, R. C. & Bartholomew, C. H. The stoichiometries of H_2 and CO adsorptions on cobalt: Effects of support and preparation. *J. Catal.* **85**, 63-77, (1984).
13. Duan, L. *et al.* Adsorption, Co-adsorption, and reactions of sulfur compounds, aromatics, olefins over Ce-exchanged Y zeolite. *J. Phys. Chem. C* **116**, 25748-2575 (2012).

14. Xue, M. *et al.* Preparation of cerium-loaded Y-zeolites for removal of organic sulfur compounds from hydrodesulfurizated gasoline and diesel oil. *J. Colloid Interface Sci.* **298**, 535-542 (2006).
15. Sexton, B. A. *et al.* An XPS and TPR study of the reduction of promoted cobalt-kieselguhr Fischer-Tropsch catalysts. *J. Catal.* **97**, 390-406 (1986).
16. Ernst, B. *et al.* Study on a cobalt silica catalyst during reduction and Fischer-Tropsch reaction: In situ EXAFS compared to XPS and XRD. *Catal. Today* **39**, 329-341(1998).
17. Moodley, D. J. *et al.* Carbon deposition as a deactivation mechanism of cobalt-based Fischer-Tropsch synthesis catalysts under realistic conditions. *Appl. Catal. A* **354**, 102-110 (2009).
18. Ferrari, A. C. & Robertson, J. Interpretation of Raman spectra of disordered and amorphous carbon. *Phys. Rev. B* **61**, 14095-14107 (2000).
19. Pimenta, M. A. *et al.* Studying disorder in graphite-based systems by Raman spectroscopy. *Phys. Chem. Chem. Phys.* **9**, 1276-1291 (2007).
20. Flory, P. J. Molecular size distribution in linear condensation polymers. *J. Am. Chem. Soc.* **58**, 1877-1885 (1936).
21. Friedel, R. A. & Anderson, R. B. Composition of synthetic liquid fuels. I. Product distribution and analysis of C_5-C_8 paraffin isomers from cobalt catalyst. *J. Am. Chem. Soc.***72**, 1212-1215(1950).
22. Zhang, Q., Kang, J. & Wang. Y. Development of novel catalysts for Fischer Tropsch synthesis: tuning the product selectivity. *ChemCatChem* **2**, 1030-1058 (2010).
23. Galvis, H. M. T. *et al.* Supported iron nanoparticles as catalysts for sustainable production of lower olefins. *Science* **335**, 835-838 (2012).